Available online at www.sciencedirect.com

ScienceDirect

Journal of Geodynamics 45 (2008) 178–190

JOURNAL OF GEODYNAMICS

http://www.elsevier.com/locate/jog

Cretaceous subduction-related volcanism in the northern Sanandaj-Sirjan Zone, Iran

Hossein Azizi[a,*], Ahmad Jahangiri[b]

[a] *Mining Department, Faculty of Engineering, University of Kurdistan, P.O. Box 66177-15175, Sanandaj, Iran*
[b] *Geology Department, Faculty of Natural Sciences, University of Tabriz, Tabriz, Iran*

Received 14 February 2007; received in revised form 7 November 2007; accepted 7 November 2007

Abstract

Cretaceous volcanic rocks (SCV) are widely developed in the northern part of the Sanandaj-Sirjan Zone, northwest Iran. Based on the mineralogy, texture and geochemical composition these rocks are divided in two main groups, the first and main one situated in the central part of the study area and the second one in the northeast. The former is dominantly basalts, andesitic basalts, and andesites and the latter comprises andesite, trachy-andesite to acidic variants, with porphyritic to microlithic porphyry and vitrophyric textures. Beside the differences between these two groups, the chemical compositions all of these rocks show a calc-alkaline affinity and enrichment in LIL elements (Rb, Ba, Th, U, and Pb) and depletion in Nb, Ti, and Zr, as evident in spider diagrams normalized to primitive mantle. The rocks are particularly enriched in Rb and depleted in Nb and Ti, as well as displaying high Rb/Sr and Rb/Ba ratios and low ratios of incompatible elements such as Nb/U (<10; range, 0.6–9), Th/U (<2), and Ba/Rb (<20). The significant U enrichment relative to neighbouring Nb and Th in the mantle-normalized variation diagram is mainly a result of source enrichment by slab-derived fluids. Significantly lower Nb/U ratios are observed in arc volcanics. These low values are generally ascribed to the strong capacity of LILE and the inability to transfer significant amounts of HFSE via slab-derived hydrous fluid. The results of geochemical modelling suggest a mantle lithospheric source that was metasomatized by fluids derived from a Neo-Tethyan subducted slab during the Middle to Late Cretaceous in the northern part Sanandaj-Sirjan Zone.

Keywords: Sanandaj-Sirjan Zone; Iran; Calc-alkaline; Volcanism; Neo-Tethyan; Subduction

1. Introduction

The Tethyan orogen formed from the collision of Eurasia with dispersed fragments of Gondwanaland (Sengor, 1984; Sengor and Natal'in, 1996). Rifting from the Late Palaeozoic to Early Mesozoic formed ribbon fragments of continental crust that broke away from the northern margin of Gondwanaland to form the Tethys Ocean. The Zagros Mountains of western Iran are part of this orogenic collage, having developed from continental separation and subsequent collision between a fragment of Gondwanaland and central Iran.

Three major tectonic elements – the Zagros Fold-Thrust Belt, the Sanandaj-Sirjan Zone, and the Urumieh-Dokhtar magmatic arc (Alavi, 1994) – are recognized in western and southwestern Iran as being related to the subduction of Neo-Tethyan oceanic crust and subsequent collision of the Arabian plate with the central Iran microplate. The Zagros Fold-Thrust Belt (ZFTB) lies on the northeastern margin of the Arabian platform and consists of a Phanerozoic succession with a stratigraphic thickness of up to 10 km that is folded into simple kilometre-scale anticlines and synclines (Stocklin, 1968). This fold belt, which is 200–300 km wide, formed in the late Cenozoic and is still tectonically active, with ongoing shortening and thickening associated with collision between the Arabian Peninsula and central Iran (Berberian, 1995).

The Sanandaj-Sirjan Zone (SSZ) is a narrow zone of highly deformed rocks located between the towns of Sirjan and Esfandagheh in the southeast and Urumieh and Sanandaj in the northwest (Mohajjel and Fergusson, 2000). The rocks in this zone are the most highly deformed of the Zagros belt, and share the NW–SE trend of surrounding structures. The zone is dominated by Mesozoic rocks; Palaeozoic rocks are generally rare, but are common in the southeast (Berberian, 1995). The SSZ is characterized by metamorphosed and complexly deformed

* Corresponding author. Tel.: +98 871 6660073; fax: +98 871 6660073.
E-mail address: Hossien_azizi@uok.ac.ir (H. Azizi).

0264-3707/$ – see front matter © 2007 Elsevier Ltd. All rights reserved.
doi:10.1016/j.jog.2007.11.001

rocks associated with abundant deformed and undeformed plutons, as well as widespread Mesozoic volcanics. The SSZ is subdivided into two parts (Eftekharnejad, 1981): the southern part consists of deformed and metamorphosed rocks of Middle to Late Triassic age; the northern part consists of numerous Upper Cretaceous intrusive and volcanic rocks as well as greenschist facies metamorphic rocks.

A belt of black- and green-coloured Cretaceous volcanic rocks occurs in the northern part of the SSZ. The belt is 5–15 km wide and 80–120 km long, striking NW–SE from Nahavand to Urmieh, parallel to the main Zagros Fault (Fig. 1). The belt appears to be the northern extent of the marginal sub-zone of the SSZ proposed by Mohajjel et al. (2003), which is characterized by Cretaceous volcanic rocks and shallow-marine sediments.

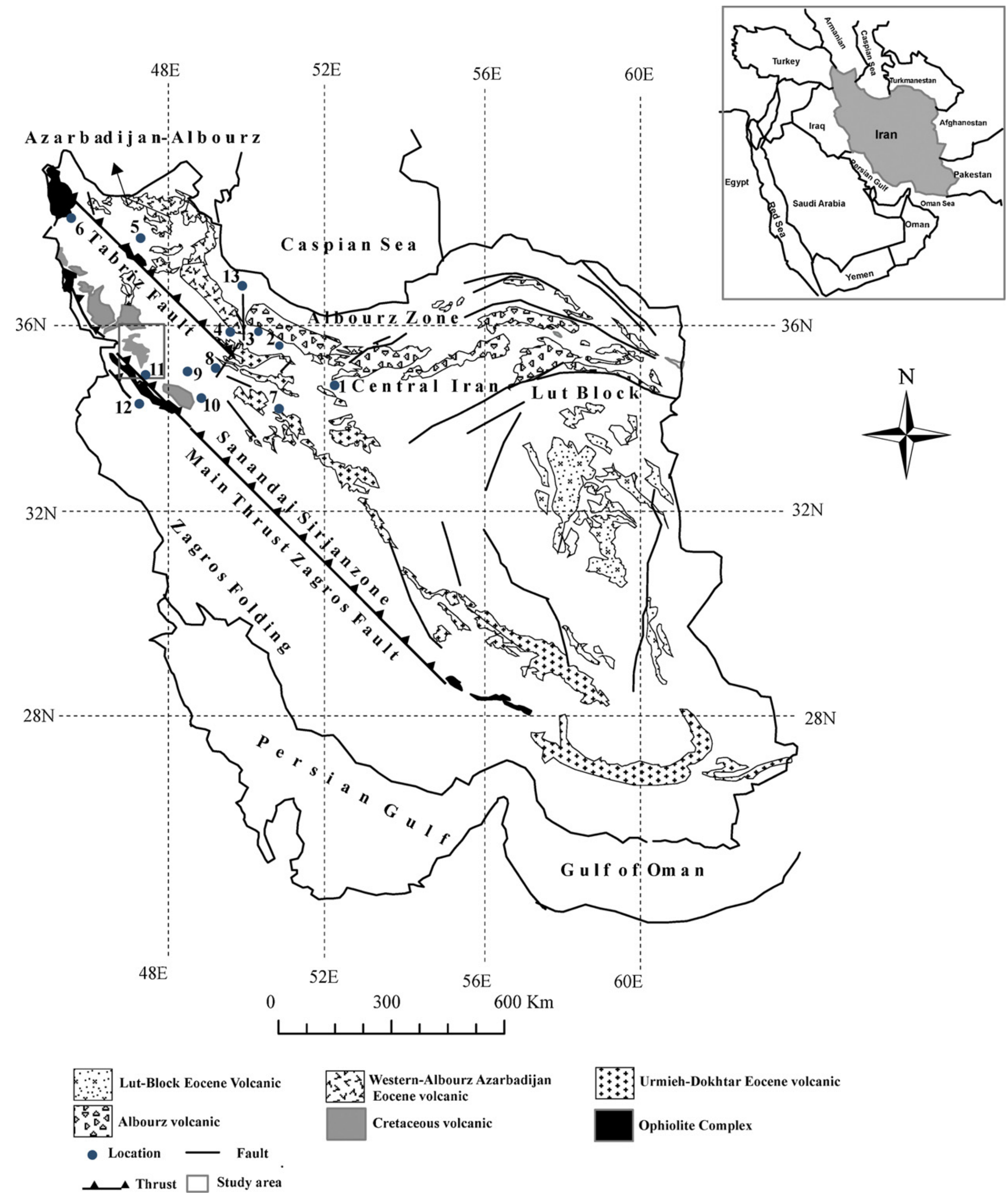

Fig. 1. Distribution of Cretaceous and Tertiary (especially Eocene) volcanic rocks and dismembered ophiolites from west to the northwest Iran. Study area is shown by box. Locality names—(1) Tehran; (2) Ghazvin; (3) Takestan; (4) Zanjan; (5) Tabriz; (6) Khoy; (7) Saveh; (8) KabodarAhang; (9) Hamadan; (10) Nahavand; (11) Sanandaj; (12) Kermanshah; (13) Rasht.

The volcanic rocks of the marginal sub-zone are interpreted to represent volcanic rocks that accumulated in a fore-arc basin located along the southwestern margin of the Urumieh-Dokhtar magmatic arc (Alavi, 1994); however, this interpretation is inconsistent with the Eocene to Pliocene age of magmatic activity in the Urumieh-Dokhtar magmatic arc (Mohajjel et al., 2003). These volcanic rocks are interbedded with detrital sediments such as black shale, sandstone, and sandy limestone to the north of Sanandaj (Zahedi et al., 1985).

The Tertiary Urmieh-Dokhtar volcanic belt trends NW–SE, parallel to the main Zagros Thrust in west Iran between the SSZ and the central Iran zone. North of Saveh, the belt can be divided by the Takestan-KabodarAhang Fault into two parts. In the present study, we refer to the southern branch of the belt as Savah-Taftan, and the northern branch as Saveh-Urmieh. The Saveh-Taftan zone is dominated by basic to intermediate volcanic rocks with a calc-alkaline to alkaline affinity.

The Albourz Tertiary volcanic belt is situated in north Iran and has an E–W orientation. This belt is divided into western and eastern parts by the N–S Rasht-Takestan Fault. The eastern part consists of basic and acidic tuff and lava with an alkaline to shoshonitic affinity (Blourian, 1994), while the western part – which we refer to as the "Albourz (Takestan)-Azarbadijan" (AA) volcanic belt – consists of andesitic to dacitic lava and many granitoid bodies with a calc-alkaline affinity (Moayyed, 2001). The AA volcanic belt is separated from the central Iranian microplate to the south by the Tabriz Fault; to the north, the belt extends into Armenia (Fig. 1).

Due to the effects of alteration and the challenging morphology of the study area, Cretaceous volcanic rocks have not been studied previously. This research is the first to investigate the geochemical and tectonic setting of these rocks. Despite a number of limitations in the present research (e.g., the absence of isotopic data and lack of structural analysis), we believe that this paper will prove to be a key work for subsequent studies in this area. We examine the detailed petrography and geochemistry of the Cretaceous volcanic rocks to understand the evolution of volcanism in the area and reconstruct the regional-scale tectonic setting of Cretaceous volcanism within the SSZ. In this paper, we use the term 'SCV' to describe the Sanandaj Cretaceous Volcanics where they occur *in situ*.

2. Regional geology

The northern part of the SSZ, termed the Sanandaj-Mahabad zone (Eftekharnejad, 1981), is located between two dismembered ophiolite complexes: the Khoy ophiolite to the east and the Kermanshah ophiolite to the west (Fig. 1). The Kermanshah ophiolite is highly dismembered, and consists of both mantle and crustal suites such as peridotite (dunite and harzburgite), cumu-

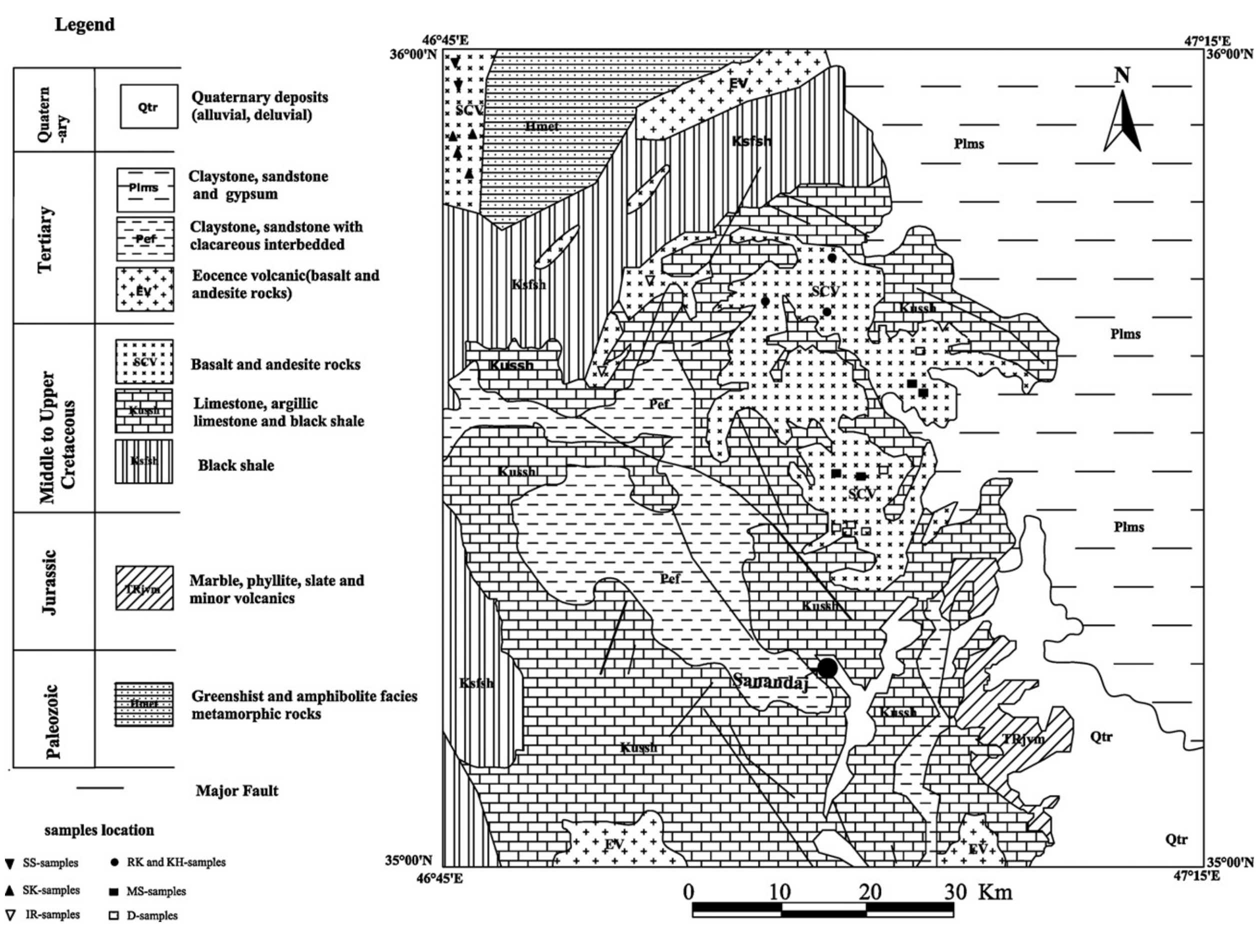

Fig. 2. Geological map of study area. Samples locations are shown in this figure.

Table 1
Major (in wt%) and trace element (in ppm) data and some element ratios from The SCV rocks in the north of the SSZ

Sample no	D1	D4	D7	D11	D12	D117	MS6	MS20	MS21	MS22
Location	35°25′16″N; 46°59′33″E	35°25′08″N; 46°59′32″E	35°25′06″N; 46°59′30″E	35°29′50″N; 47°03′37″E	35°44′15″N; 47°05′30″E	35°31′48″N; 47°01′10″E	35°27′41″N; 46°57′32″E	35°29′36″N; 47°03′18″E	35°31′48″N; 47°05′55″E	35°31′49″N; 47°05′55″E
Rock type	Andesite	Basaltic-andesite	Basaitic-andesite	Andesite	Basalt	Basaitic-andesite	Trachy-andesite	Basalt	Basalt	Andesite
SiO_2 (wt%)	56.44	55.07	52.55	55.5	50.51	54.25	53.44	49.26	50.91	54.92
TiO_2	0.77	1.02	0.83	0.7	0.55	0.74	0.72	0.78	0.817	0.8
Al_2O_3	14.22	15.09	15.49	14.61	11.88	14.23	14.41	15.48	16.62	14.15
Fe_2O_3(tot)	9.29	9.52	10.31	9.37	9.85	9.43	9.09	11.45	11.48	9.27
MnO	0.15	0.13	0.16	0.14	0.15	0.19	0.14	0.11	0.13	0.14
MgO	4.81	3.22	8.48	3.99	7.9	6.81	7.86	10.25	7.04	6.73
CaO	5.59	7.85	2.77	8.5	9.4	7.18	8.18	5.28	5.84	5.87
Na_2O	2.88	4.3	2.36	1.53	1.26	2.22	1.33	0.92	3.69	2.65
K_2O	2.4	1.32	2.23	2.84	1.06	0.05	0.98	1.07	1.14	1.03
P_2O_5	0.12	0.21	0.18	0.14	0.14	0.18	0.15	0.14	0.19	0.21
LOI	2.96	2.29	4.47	2.24	7.02	4.4	3.22	5.05	3.77	3.6
Ba (ppm)	447	232	442	572	574	28	373	434	505	501
Rb	52	24	45	53	25	8	25	29	28	28
Sr	452	231	188	951	367	318	410	408	380	379
Y	17	15	15	15	13	13	13	13	13	14
Zr	98	114	71	74	54	81	61	65	69	70
Nb	5	9	6	3	4	7	3	2	1	3
Th	2	1	2	2	6	2	3	2	4	7
Pb	7	10	7	3	8	13	10	12	6	3
Zn	83	73	82	70	69	82	70	76	76	85
Cu	31	73	91	35	50	36	24	30	58	60
Ni	15	21	13	19	80	8	38	41	15	31
V	147	156	196	144	163	158	144	186	165	160
Cr	7	13	12	36	252	16	73	55	65	60
Co	23	5	29	23	33	22	18	32	20	26
U	1	1	2	1	4	1	2	1	1	5
La	12	16.3	22.7	18.6	15.5	15	14.9	12.9	15.9	15.2
Ce	24.6	33.7	46.3	36.8	30.6	32.2	29.3	32.1	32.1	31.4
Pr	3.79	5.19	6.97	5.53	4.52	4.93	4.43	4.55	5.07	4.82
Nd	15.9	20.6	28.3	22.2	18.2	19.9	18.2	18.3	20.6	19.3
Sm	3.47	4.29	5.76	4.4	3.68	3.82	3.67	3.8	3.93	3.86
Eu	1.04	1.32	1.64	1.34	1.21	1.07	1.22	1.18	1.19	1.18
Gd	3.04	3.7	4.38	3.33	2.78	2.92	2.91	3	3.25	3.02
Tb	0.63	0.74	0.79	0.62	0.54	0.58	0.54	0.55	0.61	0.6
Dy	4.05	4.8	4.65	3.87	3.07	3.75	3.41	3.41	3.69	3.67
Ho	0.71	0.81	0.78	0.68	0.52	0.63	0.56	0.56	0.63	0.61
Er	2.25	2.58	2.4	2.11	1.6	2.11	1.89	1.77	1.97	1.96
Tm	0.32	0.36	0.33	0.29	0.23	0.26	0.27	0.23	0.27	0.26
Yb	2.2	2.48	2.15	2.11	1.61	1.92	1.82	1.66	1.93	1.86
Lu	0.29	0.34	0.3	0.29	0.22	0.26	0.27	0.2	0.24	0.24
Th/U	2	1	1	2	1.5	2	1.5	2	4	1.4
Ba/Rb	8.6	9.66	9.82	10.79	22.96	3.5	14.92	14.96	18.03	17.89
Nb/U	5	9	3	3	1	7	1.5	2	1	0.6
Ce/Pb	3.51	3.77	6.61	12.26	3.82	2.47	2.93	2.67	5.35	10.46
Th/La	0.16	0.06	0.08	0.1	0.0.38	0.13	0.2	0.15	0.25	0.46
Th/Nb	0.4	0.11	0.33	0.66	1.5	0.28	1	1	4	2.33
Zr/Nb	19.6	12.7	8-Nov	24.66	13.5	11.57	20.3	32.5	69	23.33
La/Nb	2.4	1.81	3.76	6.2	3.87	2.14	4.96	6.45	15.9	5.06
Mg#	57.88	45.29	68	53.3	66.97	65.43	69.11	69.07	58.72	65.91

Table 1 (*Continued*)

Sample no.	IR1	IR2	KH1	KH2	RK3	SK1*	SK2*	SK3*	SK4*	SS1*
Location	35°35′51″N; 46°51′32″E	35°37′49″N; 46°53′57″E	35°46′10″N; 46°54′43″E	35°45′15″N; 46°54′52″E	35°45′55″N; 46°55′30″E	35°55′10″N; 46°45′17″E	35°55′15″N; 46°45′12″E	35°57′55″N; 46°45′25″E	35°54′55″N; 46°45′20″E	35°57′12″N; 46°45′06″E
Rock type	Andesite	Bastic-andesite	Basalt	Basaltic-andesite	Basalt	Trachy-andesite	Trachy-andesite	Basatic-andesite	Basaltic-andesite	Trachy-andesite
SiO_2 (wt%)	54.9	50.72	51.24	53.83	47.77	62.34	62.27	52.52	54.22	59.4
TiO_2	0.79	1.07	1.59	1.86	0.6	0.63	0.89	1.29	1.06	0.636
Al_2O_3	13.87	14.82	11.5	11.4	11.93	15.47	16.41	16.3	15.34	12.6
Fe_2O_3(tot)	12.51	12.45	11.59	12.52	10.73	5.03	5.88	10.18	8.9	5.57
MnO	0.101	0.24	0.166	0.223	0.193	0.041	0.034	0.151	0.17	0.04
MgO	5.16	6.11	3.75	5.54	5.39	2.86	2.84	4.18	3.02	2.12
CaO	5.58	4.88	11.18	7.94	12.11	4.09	1.06	7.72	8.78	8.32
Na_2O	1.22	1.46	2.61	2.03	1.07	3.91	5.91	2.16	1.59	5.7
K_2O	2.35	3.46	0.19	0.95	0.95	2.9	2.02	2.75	2.73	0.05
P_2O_5	0.18	0.25	0.24	0.32	0.24	0.42	0.46	0.28	0.25	0.39
LOI	2.97	4.25	5.68	2.89	8.4	1.91	1.86	2.17	3.32	4.68
Ba (ppm)	757	1638	192	304	567	1308	735	954	753	82
Rb	56	79	12	19	30	72	39	47	56	14
Sr	293	145	427	391	485	1724	1198	1184	697	378
Y	18	19	21	21	20	12	19	16	15	16
Zr	90	84	143	143	131	347	314	202	172	196
Nb	5	5	12	20	7	38	36	27	25	34
Th	6	8	6	6	8	9	5	7	6	9
Pb	10	6	3	3	7	8	22	92	2	2
Zn	47	94	69	61		67	63	124	75	47
Cu	47	37	46	48	42	32	32	64	67	28
Ni	38	56	52	53	47	55	59	34	36	145
V	271	246	233	253	180	89	112	252	244	73
Cr	29	57	35	42	33	35	47	29	29	92
Co	29	28	29	31	22	23	10	27	14	13
U	3	2	3	5	4	5	4	5	5	6
La	13.7	11.9	17	19	33.1	72	27.9	26.5	31.4	52
Ce	30	27	37.2	36.9	61.9	114	45.2	58.4	66.6	95.6
Pr	3.65	2.95	3.83	3.41	5.37	8.57	3.73	6.68	6.78	8.42
Nd	18.9	18.8	18	19.1	29.9	36.1	16.6	30.4	38.8	43.6
Sm	2.41	3.18	4.07	3.45	4.62	4.45	2.04	5.54	5.3	4.05
Eu	1.19	1.62	1.16	1.15	1.29	1.45	0.63	1.85	1.7	1.13
Gd	3.79	4.29	4.21	3.98	4.66	3.23	1.48	4.9	5.35	3.23
Tb	0.6	0.63	0.71	0.68	0.71	0.44	0.21	0.7	0.71	0.38
Dy	3.18	3.02	3.66	3.05	2.79	1.72	0.79	3.44	3.01	1.45
Ho	0.67	0.62	0.67	0.6	0.53	0.27	0.14	0.61	0.57	0.24
Er	2.13	2.12	2.2	2.06	1.79	0.89	0.48	1.79	1.91	0.77
Tm	0.28	0.28	0.3	0.29	0.23	0.13	0.07	0.22	0.23	0.09
Yb	1.89	1.67	2.16	2.06	1.51	0.89	0.46	1.53	1.44	0.52
Lu	0.24	0.18	0.27	0.25	0.16	0.11	0.06	0.19	0.16	0.07
Th/U	2	4	2	1.2	2	1.8	1.25	1.4	1.2	1.5
Ba/Rb	13.51	20.73	16	16	18.9	18.16	18.84	20.29	13.44	5.85
Nb/U	1.66	2.5	4	4	1.75	7.6	9	5.4	5	5.66
Ce/Pb	3	4.5	12.4	12.3	8.84	14.25	2.05	0.63	33.3	47.8
Th/La	0.43	0.67	0.35	0.31	0.24	0.12	0.17	0.26	0.19	0.18
Th/Nb	1.2	1.6	0.5	0.3	1.14	0.23	0.13	0.25	0.24	0.26
Zr/Nb	18	16.8	12	7.25	18.71	9.13	8.7	7.48	6.88	5.76
La/Nb	2.74	2.38	1.41	0.95	4.72	1.89	0.77	0.98	1.25	1.52
Mg#	48.69	55.31	46.89	54.75	55.55	66.35	62.04	53.11	48.81	55.25

Group 2 is showed by star (*). All samples are lava.

late gabbro and diorite, and a volcanic sequence that ranges in composition from sub-alkaline basalt to alkaline basalt and trachyte. Associated sedimentary rocks include a variety of Upper Triassic to Lower Cretaceous deep- and shallow-water sedimentary rocks.

Geochemical data clearly distinguish two distinct types of basalt (Ghazi and Hassanipak, 1999; after Ghasemi and Talbot, 2006): sub-alkaline basalt with an island arc affinity and alkaline basalt with a typical oceanic island signature. The Kermanshah ophiolites therefore formed in both an island arc environment and an intra-plate oceanic island environment before being thrust over Lower Triassic–Upper limestone of the Cretaceous Bisoton seamount during the Maastrichtian (Lippard et al., 1986). Palaeocene volcanism and Eocene shallow-water limestone unconformably overlie the Kermanshah ophiolite (Braud, 1987).

The Khoy ophiolite has been studied by many researchers (e.g., Ghazi and Hassanipak, 1999), but recent studies by Azizi (2002) and Azizi et al. (2006) reveal that the complex consists of pillow lava, sheeted dykes, massive gabbro, and lherzolite, along with lesser harzburgite and pelagic sediments. The complex is Lherzolite-Type (LOT), formed in a back-arc basin in the Late Cretaceous and obducted during the Eocene.

Cretaceous sequences in the Sanandaj region are locally different to those in other parts of the SSZ. A thick (2000–3000 m) sequence of sediments consists of shallow-marine detrital sediment overlain by marine sediments interbedded with volcanic rocks. This sequence is repeated over at least three cycles (Zahedi et al., 1985). The high rate of subsidence in the Sanandaj region led to a short interval over which pelagic sediments were deposited in the basin. This basin could well be interpreted as a local pull-part basin that developed along a major strike-slip fault that initiated and developed during an oblique convergence event (Sengor, 1990; Azizi et al., 2005).

Permian schist and marble are the oldest exposed rocks in the north and northwest of the study area (Fig. 2). The Mesozoic sequence in this area consists of sandy limestone, shale, and crystalline limestone intercalated with Jurassic volcanics, and Cretaceous basic to intermediate volcanic rocks interbedded with dark grey shale. The Mesozoic sequence is well exposed to the north of Sanandaj, where it unconformably overlies a red basal conglomerate of Eocene age, which, in turn, conformably overlies Oligocene limestone. The area west of Sanandaj contains exposures of sandy shale with limestone lenses and sandy limestone interbedded with Cretaceous–Paleocene volcanics.

3. Petrography

The SCV rocks are divided into two groups; the first group has green to black colour representing the main type the SCV rocks and the second group is purple to grey in colour as distinguished in the field. The second group is separated by the first one by outcropping in the northern part of the SCV. Study of 117 thin section shows that these two groups present some differences in texture and mineralogy.

Group 1 comprises basalt, andesitic basalt, and andesite that are fine-grained and display porphyritic to microlithic porphyritic textures. Phenocrysts include altered plagioclase and clinopyroxene up to 1 mm in size. Plagioclase phenocrysts are subhedral to anhedral and partly altered to epidote and calcite. The microcrystalline matrix is dominated by small microliths of plagioclase. Plagioclase is up 40–60% in the basaltic to andesitic rocks. The clinopyroxene, which is up 10–20% of the rock volume, occurs as euhedral or subhedral augite phenocrysts.

Features such as poikilitic texture and embayments along the rims of clinopyroxene phenocrysts indicate the instability of these minerals during ascent through the crust. Rare hornblende, biotite, and magnetite are also observed in these rocks. Secondary zeolite minerals are present in the voids.

Group 2 has trachytic, trachyte-porphyric, ignimbrite textures and present hornblende as the main mineral. This group comprises andesite, trachy-andesite, trachyte and silicic members. Plagioclase and K-feldspar are the main minerals as phenocrysts and in the matrix, and are mostly replaced with epidote, white mica and clay minerals. Hornblende is a minor mineral and it is replaced with opacite in the rim and along the cleavages; also magnetite and titanite are accessory minerals in this group. The result of petrographic is shown in Appendix A.

4. Geochemistry

4.1. Analytical methods

Major elements were determined by X-ray fluorescence spectrometry (XRF) of fused glass pellets at the AMDEL Laboratory, Adelaide, Australia. All trace elements, including rare earth elements (REE), were analysed using a PE Elan6000 inductively coupled plasma mass spectrometer (ICP-MS) at the AMDEL Laboratory. For ICP-MS analyses, pure elemental standards were used for external calibration. The detection limit was 0.01% for all major element oxides and 0.5–1 ppm for rare earth elements.

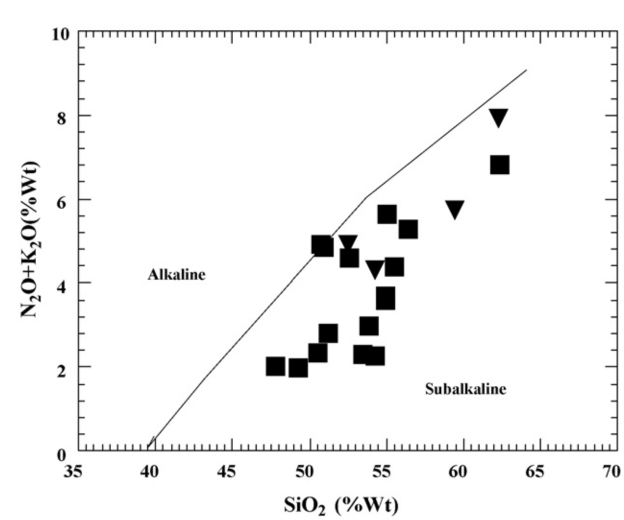

Fig. 3. Total alkalis vs. silica diagram. The SCV samples plot in sub-alkaline field. Rectangle and filled triangle shows Groups 1 and 2, respectively.

The major and trace element compositions of the SCV rocks are presented in Table 1. Samples D12, MS20, MS21, IR1, IR2, KH1, and KH2 are basaltic; all of the others are basaltic andesite, andesite and trachy-andesite. Although the samples are altered, most show only minor (>4 wt%) loss on ignition.

4.2. Major elements

Although the analysed volcanic rocks are susceptible to alteration, the major and trace element compositions of the least-altered samples are informative in terms of the primary composition, provided that due care is taken in the selection of elements and element ratios.

The SCV rocks are all basic to intermediate (SiO_2 content of 48–62 wt%) and possess remarkably high Al_2O_3 content (12–17 wt%) and low K_2O content (<2.8 wt%); the Na_2O/K_2O ratio is as high as 1. Most of the analysed mafic rocks do not have a primary magmatic composition; instead, they are clearly evolved mafic volcanic rocks that experienced fractionation of olivine, clinopyroxene, and/or plagioclase.

In the $Na_2O + K_2O$ versus SiO_2 diagram (Irvine and Baragar, 1971), all of the SCV rocks plot in the sub-alkaline field (Fig. 3). The abundance of TiO_2 varies between 0.6 and 2 wt% (generally less than 1 wt%); P_2O_5 content ranges from 0.1 to 0.5 wt%; and both oxides display enrichment with decreasing MgO. TiO_2 and FeO (total) contents increase slightly with decreasing MgO,

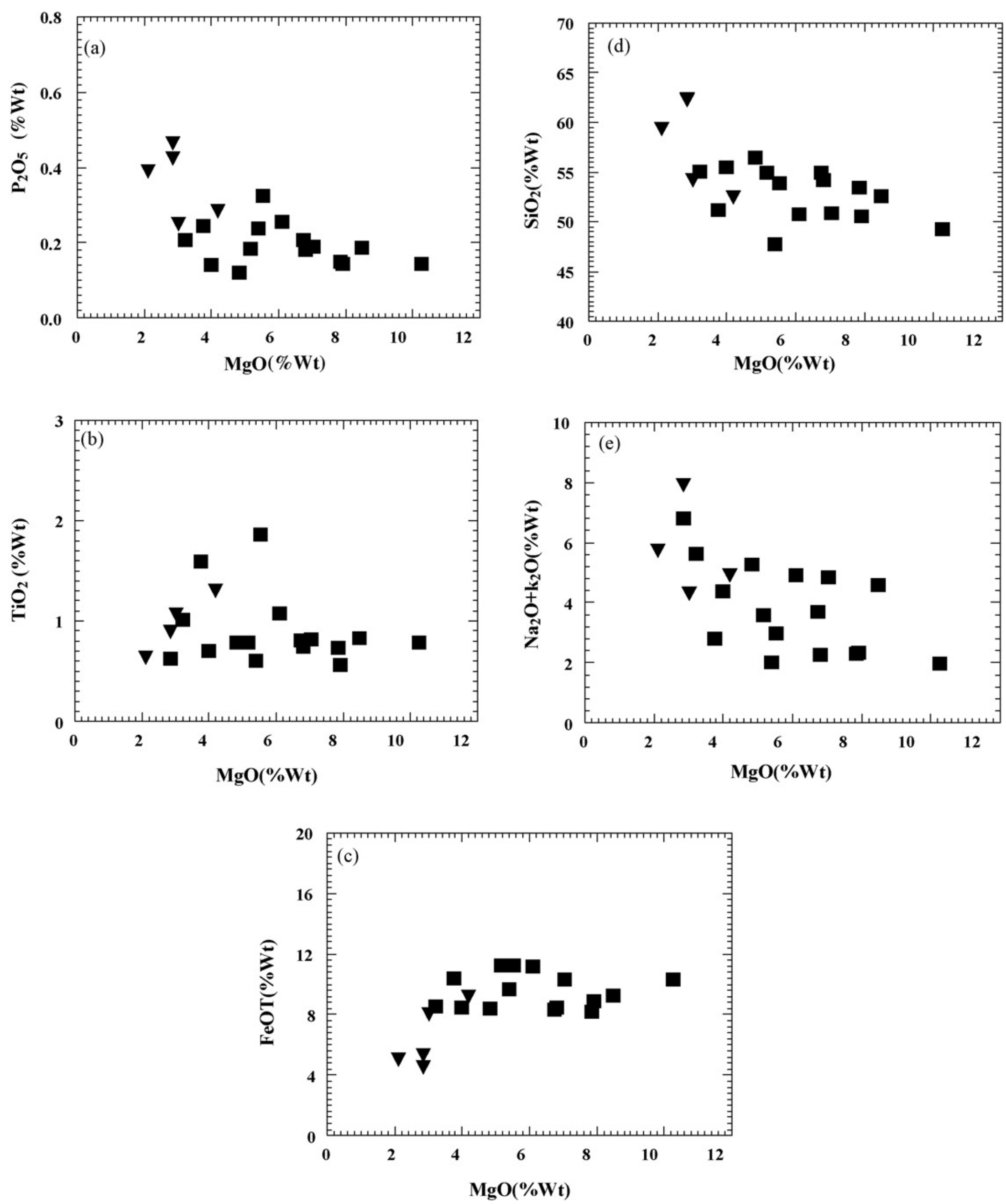

Fig. 4. Variation of major elements (wt%) vs. MgO (wt%) for the SCV samples. Symbols are the same as in Fig. 3.

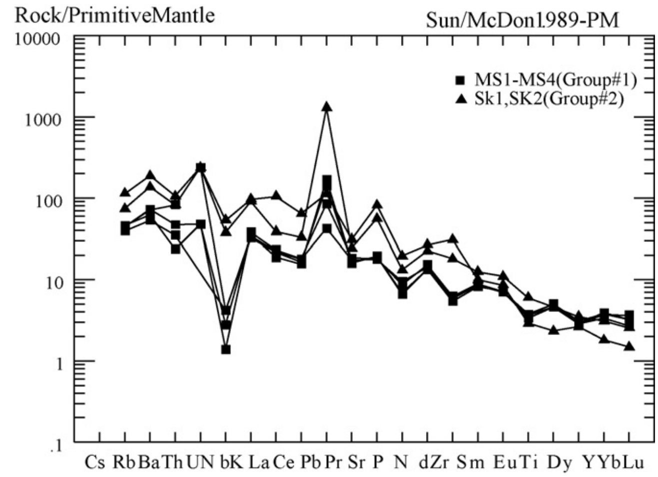

Fig. 5. The SCV basalt and basaltic andesite rocks normalized with primitive mantle (normalized data from Sun and McDonough, 1989). Group 2 has higher Nb, Pb and Sr in comparison with Group 1. Symbols are the same as in Fig. 3.

and SiO_2 and alkaline elements ($Na_2O + K_2O$) show a negative correlation with MgO (Fig. 4a–e).

4.3. Trace elements

The most representative rocks of Group 1 (MS1–4) and of Group 2 (SK1, SK2) are normalized to primitive mantle (Sun and McDonough, 1989). The SCV rocks are enriched in LILE (e.g., Rb, Ba, Th, U, and Pb), depleted in HFSE (e.g., Nb, Ti), and relatively depleted in HREE (Lu, Yb < 2, Tm < 1) (Fig. 5). There are some differences between these two groups. Group 2 has higher Sr, Pb, Nb and LILE in comparison to Group 1.

Most of the basaltic rocks from the SCV are characterized by much higher Th/Nb (1.14–4) and Th/La (0.15–0.67) values and low La/Nb (0.77–15) values than normal MORB (N-MORB; 0.071, 0.067, and 1.07, respectively; Weaver, 1991).

Pearce (1983) and Pearce and Peate (1995) suggested that the geochemical contributions of mantle versus subducted plate reservoirs during the petrogenesis of arc basalt can be determined from a plot of M/Yb versus Nb/Yb, where M is the element under consideration. Therefore, we assessed the relative contributions of source composition and subduction component to the REE and HFSE contents of the SCV rocks by plotting similar diagrams with M represented by a REE or HFSE element (Fig. 6). In the case that neither Nb nor Yb are added to the mantle wedge within subduction-related fluxes, the variable addition of an M-enriched slab component to a mantle of constant composition should result in M/Yb values that differ from those of mantle-derived oceanic basalt compositions (i.e., the mantle array in Fig. 6). The amount of M/Yb displacement from the mantle array should be dependent on the magnitude of the contribution of subduction-related components and the degree of enrichment or depletion of the mantle source (Pearce, 1983; Pearce and Peate, 1995).

A qualitative estimate of the contribution of slab-derived components can therefore be made from these diagrams based on the deviation of observed M/Yb ratios from the mantle value and in particular the mantle-OIB baseline value defined by the average MORB and OIB values (Sun and McDonough, 1989). The detection limit (upper bound of the mantle array) generally lies at a subduction contribution of about 20–30% (Pearce et al., 1995). The M/Yb versus Nb/Yb trends for SCV lava tend to exhibit individual arrays sub-parallel to the MORB-OIB trends, possibly reflecting local variations in source heterogeneity and/or melting ranges (Fig. 6). Also low ratios of Nb/U and Ce/Pb indicate a fluid-dominated metasomatic event coupled with a 10–20% contribution by average sediments of the mantle source region.

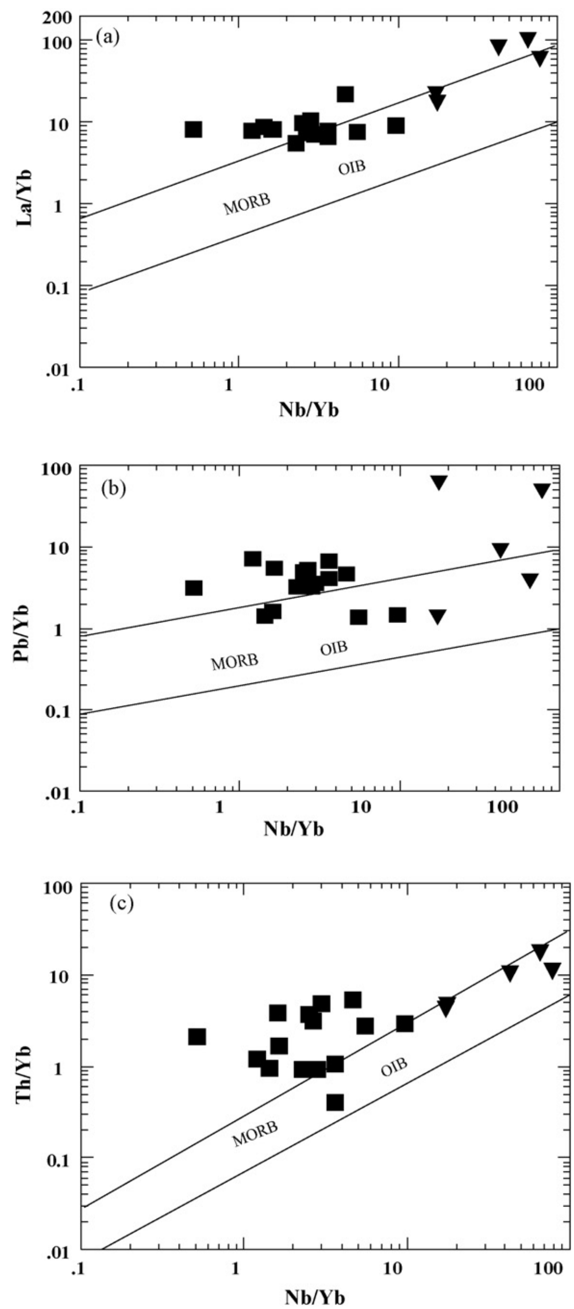

Fig. 6. Plots of M/Yb vs. Nb/Yb for the SCV basalt to andesite rocks, where M is either a HFSE and Pb or REE. Symbols are the same as in Fig. 3.

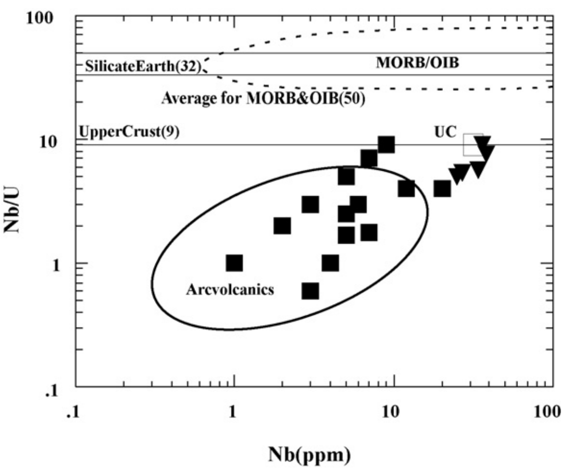

Fig. 7. Plot of Nb/U vs. Nb (ppm). Ratios for the MORB/OIB, bulk silicate earth and upper continental crust are from Hofmann et al. (1986), McDonough et al. (1992), McDonough and Sun (1995) and Rudnick and Fountain (1995). Fields for MOIB/OIB and arc volcanics are compiled from Chung et al. (2001). In this figure Group 1 rocks plot in volcanic arc fields, but Group 2 rocks are plotted nearby the upper crust field. Probably this situation can be explained by origin differences or crustal contamination. Symbols are the same as in Fig. 3.

The SCV rocks are particularly enriched in Rb and depleted in Nb and Ti; however, certain incompatible element ratios are difficult to reconcile with sediment contamination. These include Nb/U < 10 (0.6–9 for SCV rocks and 1–5.4 for basaltic rocks), Ce/Pb < 12, Th/U < 2, and Ba/Rb < 20 (Table 1). All of these ratios are significantly lower than the estimated typical values for continental crust (e.g., Taylor and McLennan, 1985) and the mantle (Hofmann, 1988; Sun and McDonough, 1989; McDonough and Sun, 1995). Given the general acceptance that igneous processes in the mantle have only a minimal effect on the fractionation of these elemental ratios, an alternative type of non-magmatic enriched is required. On the basis of mineral–aqueous fluid experiments (Brenan et al., 1995; Keppler, 1996; Ayers, 1998), we suggest that to a fluid phase derived from the neighbouring Neo-Tethyan slab might have acted as such an enrichment agent.

The similar bulk solid/melt partition coefficients of Nb and U (Hofmann, 1988; Sun and McDonough, 1989) mean that they are not significantly fractionated during mantle melting processes; consequently, melt compositions reflect the approximate Nb/U ratios of the mantle sources. For the SCV rocks, their significant U enrichment relative to neighbouring Nb and Th in the mantle-normalized variation diagram (Fig. 5; Nb/U < 10 and Th/U < 2) is mainly a result of source enrichment by slab-derived fluids. Significantly lower Nb/U ratios are observed in arc volcanics (Fig. 7), different from oceanic basalts that show a nearly constant Nb/U ratio of 50 (Hofmann et al., 1986); these values are different from the values estimated for bulk silicate earth (Nb/U = 32; McDonough and Sun, 1995) and the upper continental crust (Nb/U = 9; Rudnick and Fountain, 1995). Such as a low range of Nb/U values is similar to that calculated for subduction-zone fluids (0.15–0.3; Keppler, 1996; Ayers, 1998). These low values are generally ascribed to the strong capacity of LILE and the inability to transfer significant amounts of HFSE via slab-derived hydrous fluid. HFSE are more likely to be stored in phases such as rutile and/or ilmenite, which may persist in the subducted slab (Ryerson and Watson, 1987; Chung et al., 2001).

Experiments involving the partitioning of U and Th between minerals and aqueous fluid (Brenan et al., 1995; Keppler, 1996; Ayers, 1998) reveal that U is preferentially transported, relative to Th, from the subducting slab to the mantle wedge. Thus, a significant fractionation of Th/U could occur during dehydration processes at convergent margins. The SCV lava also shows remarkable enrichment in Pb (Fig. 5). In the fluid-modified mantle region, enrichment factors for Pb are therefore greater than those for K and Ba and similar to that for Rb (Tatsumi et al., 1986).

5. Discussion

5.1. Arc-related origin of the SCV rocks

In many ways, the basaltic rocks of the SCV are similar to those of mature island arcs/active continental margins. All of the SCV basalt and basaltic andesite rocks (Group 1) plot in the calc-alkaline continental arc and oceanic arc fields in a Nb/Yb versus Th/Yb diagram (Fig. 8), with most plotting in the continental arc field.

The intermediate to acidic term (Group 2) of The SCV rocks are generally calc alkaline, oxidized, wet (hydrous phenocrysts are typical), Sr- and Al-rich, and Fe-poor (SK samples; Table 1). These silicic rocks are interpreted to have been derived from mafic parent magmas generated by dehydration of oceanic lithosphere and melting in the wedge of mantle above a subduction zone.

These two groups have similar trends in major, minor and trace elements showing negative Nb, positive Sr and Pb anomalies. But there are some differences. High Ba, Zr and an absence

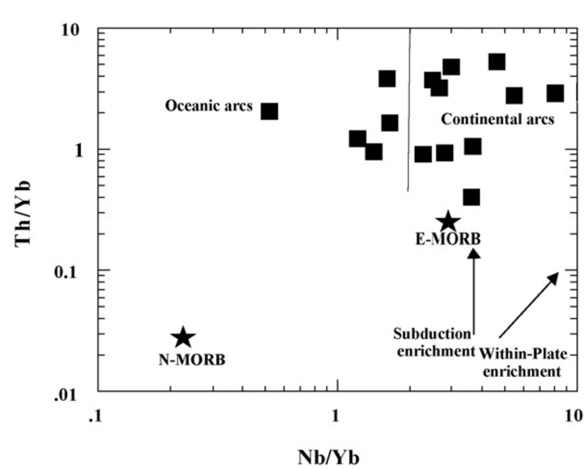

Fig. 8. Plot of Nb/Yb vs. Th/Yb for the SCV mafic to intermediate rocks. N-MORB and E-MORB values are from Sun and McDonough (1989). In this figure we plotted basaltic and basaltic andesitic rocks from Group 1 and they occupy the active margin field (continental and oceanic arcs). Since Group 2 is more silica enriched, they could not be plotted in this diagram. Symbols are the same as in Fig. 3.

of large negative Eu anomalies on normalized trace element diagrams are observed in Group 2 (Fig. 5). Such anomalies are common in Group 2 as the result of the extended fractionation of plagioclase, sanidine, and to some extent biotite. Although this group has high concentrations of high field strength elements like Ti, Zr, and Nb (Fig. 5, SK samples), they have small but distinctive negative Nb anomalies. In addition, two of the most notable trace element differences (Sr and Pb) between the two groups are related to variations in source hydration. High concentrations of both elements in the hydrous magmas of the SCV may be the result of their solubility in aqueous fluids.

Dehydration of a subducting slab of oceanic lithosphere is commonly thought to create Sr and Pb-rich fluids that rise into the overlying mantle wedge. As noted earlier, partial melting in this fluid-soaked wedge probably produced the mafic magmas that were parental to the andesite to silicic suite of the SCV. Moreover, the enhanced solubility of plagioclase in wet magma retards the depletion of Sr from the evolving magma. We assume that magma mixing, large proportions of crustal assimilation, and polybaric crystal fractionation were all important processes in generating the variety of basic to intermediate magmas erupted during Cretaceous magmatism; however, this needs further studies.

5.2. *Tectonic setting*

A difference of opinion exists in the literature concerning the timing of the closure of the Neo-Tethyan Ocean along the Zagros suture. Some authors propose a Late Cretaceous timing for continental collision, consistent with thrusting of the Neyriz and Kermanshah ophiolites over Upper Cretaceous sediments during the Maastrichtian (Berberian and King, 1981; Lippard et al., 1986; Berberian, 1995; Alavi, 1994). The alternative view is that continental collision along the Zagros suture occurred in the Miocene (Sengor et al., 1993; Sengor and Natal'in, 1996). Recent studies have proposed the existence of two parallel NE-dipping Neo-Tethyan subduction zones as part of the tectonic evolution of the Neo-Tethyan Ocean in the Iran region (e.g., Moayyed, 2001; Shahabpour, 2005; Ghasemi and Talbot, 2006). This view is based on extensive subduction-related magmatic activity within the Eocene–Pliocene Urumieh-Dokhtar magmatic arc and the occurrence of two parallel belts of ophiolite complexes: the Kermanshah ophiolite to the west and the Shahr Babak-Baft, Neyriz, ophiolites to the SE of the SSZ.

Rifting along the southeastern margin of the Afro-Arabian plate was initiated during the Permian. Extension was followed by Late Permian basaltic volcanic activity along the SSZ (Stampfli et al., 2001). The extensional event continued with

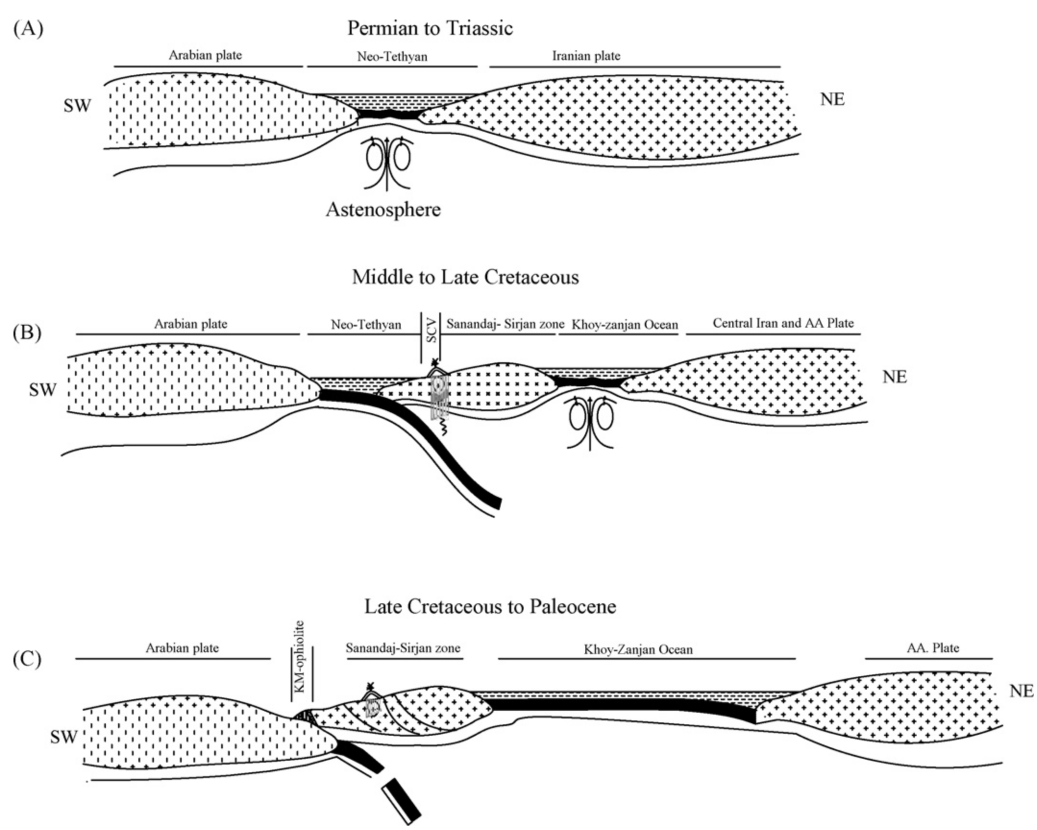

Fig. 9. Proposed model for evolution of the NW Iran. (A) Drifted Iranian plate (include SSZ and central Iran) from Arabian plate in Permian to Triassic. (B) Subduction of Neo-Tethyan oceanic plate beneath the SSZ and generation of the SCV in active margin of the SSZ and developing a new fracture with NW–SE direction in the east of the SSZ which separated it from the central Iran (C.I.) and Albourz-Azarbadijan (AA) plate in the middle to late Cretaceous probably. (C) Collision of Arabian plate with the SSZ and obuduction of NZ-ophiolite (such as Kermanshah) and developing of Khoy-Zanjan narrow oceanic crust in the upper Cretaceous-Paleocene.

the deposition of radiolarites, pelagic carbonates, and a magmatic episode that produced mafic alkaline to MORB volcanic rocks (Ricou, 1994). Extension and volcanic activity led to the generation of Neo-Tethyan Ocean crust between the SSZ and the Arabian plate. The western margin of the SSZ became active during the Early Cretaceous and oceanic crust began to be subducted beneath the SSZ during the Early to Late Cretaceous (Nowroozi, 1971; Takin, 1972; Berberian and Berberian, 1981; Moinevaziri, 1985; Alavi, 1994), leading to the obduction of a number of Neo-Tethyan oceanic slivers (Kermanshah ophiolite) over the Arabian passive continental margin in the Late Cretaceous (Turonian to Campanian; Alavi, 1994) and collision of the Arabian and Iranian plates (SSZ Plate). The subduction of Neo-Tethyan oceanic crust and the dehydration of subducted crust and slab sediments led to the metasomatism of the mantle wedge beneath the SSZ. Partial melting of the metasomatized mantle (which had a spinel- to garnet-bearing peridotite composition) then led to calc-alkaline magmatism within the SCV and the formation of a magmatic arc system north of the SSZ.

Contemporaneous with steep NE-directed subduction during the final collision, a new fracture (the Zagros Thrust) formed parallel to the Neo-Tethyan fracture in the east of the SSZ. This new structure trended NW–SE and separated the northern part of the SSZ from central Iran and the Albourz-Azerbadijan plate, probably in the Late Cretaceous. It developed further and created a narrow zone of oceanic crust (which we term the Khoy-Zanjan oceanic basin) that was subducted beneath the Albourz-Azerbadijan plate in the Eocene (probably Early Eocene); this event led to the formation of the AA volcanic belt north of the Tabriz Fault or south of the Albourz-Azerbadijan plate. The Khoy ophiolite and some of the mafic and ultramafic bodies that outcrop along the Tabriz Fault are relicts of this oceanic crust that was situated east of the SSZ (passive margin). The entire tectonic history is summarized in Fig. 9.

6. Conclusion

The overall petrography, petrology, and geochemistry of the SCV rocks to the north of Sanandaj in Kurdistan province, Iran, lead to the conclusion that the SCV lavas were derived from a lithospheric mantle source. The data indicate that the lithospheric mantle was affected by slab-related hydrous fluid resulting from the nearby subduction of the Neo-Tethyan Ocean under the SSZ. The fluid-related metasomatism was pervasive, and eventually led to the mantle becoming hybridized and highly enriched in compatible elements, with unusual elemental ratios. In agreement with published mineral–fluid experimental data, we interpret that the metasomatized mantle source for SCV lavas had highly fractionated ratios of Rb/Cs, Nb/U, Ce/Pb, Rb/Ba, and Th/U. These observations support the hypothesis of dehydration associated with slab subduction at a convergent margin.

Finally, it is important to acknowledge that the extensive development of volcanic and plutonic rocks of contrasting composition and tectonic settings in Iran cannot be interpreted in terms of a single, simple subduction zone. We believe that further understanding of the tectono-magmatic evolution of Iran requires additional chemical and isotopic analyses.

Acknowledgements

We acknowledge support from Kurdistan University. We thank Professor H. Moeinvaziri for help with microscopy and geochemical interpretations, Mr. Hamdollahi for technical assistance, and the AMDEL Laboratory for XRF and ICP analyses. We are grateful to Randell Stephenson, Chief Editor of the *Journal of Geodynamics*, and three anonymous reviewers for constructive suggestions and comments.

Appendix A. Petrography table

Sample	Rock type	Texture	Major minerals (phenocrysts)	Minor minerals (phenocrysts)	Matrix minerals	Alteration minerals	Remarks
D1	Andesite	Porphyric	Pl, Cpx	Kf	Pl, Cpx, Qtz, Mt	Chl, Cal, Ep, Ze	Pl and Cpx are idiomorphic to sub-idiomorphic
D4	Basaltic andesite	Microlite-porphyric amygdaloidal	–	Pl, Mt	Pl, Cpx, Mt	Ze,Cal, Ep, Chl, Ab Act	Ze and Chl are amygdales
D7	Basaltic andesite	Microlite-porphyric	Pl	Kf	Pl, Cpx, Mt	Ep, Chl, Cal, Ab	Mafic mineral is replaced by Chl
D11	Andesite	Porphyric	Cpx, Pl	–	Pl, Cpx, Mt	Cal, Chl, Ep	Matrix is cryptocrystalline, Cpx has sieve texture
D12	Andesite	Porphyric	Cpx, Pl	–	Pl, Cpx, Mt	Cal, Chl, Ep	The same as D11
D117	Basaltic andesite	Porphyric	PL, Kf	Cpx, Mt	PL, Kf	Ep, Act, Cal, Chl	Ep is high
MS6	Trachy-andesite	Porphyric	Cpx, Pl	Mt	Pl, Cpx	Ep, Chl, Cal, Ze	Phenocrysts value > 70% matrix is cryptocrystalline. Alteration intensity is high
MS20	Basalt	Porphyric	Pl, Cpx	Kf	Pl	Ep, Chl, Cal, Ab	Matrix is cryptocrystalline with some glass
MS21	Basalt	Porphyric, amygdaloidal	Pl, Cpx	Kf	Pl, Cpx, Mt	CC, Ep, Chl, Ab, Act	
MS22	Andesite	Microlite-porphyric	Pl, Cpx	Kf	PL, Cpx	Ep, Ab, Cal, Chl	
IR1	Andesite	Porphyric	Pl, Cpx, Kf	Mt	Pl, Cpx, Qtz	Ep, Act, Cal, Chl	Alteration intensity is high
IR2	Basaltic andesite	Trachyte-porphyric	PL	Cpx, Mt, Hbl	Pl	Ab, Act, Chl, Cal, Ep	Phenocrysts value < 15% mafic phenocryts completely alterated
KH1	Basalt	Microlite-porphyric, amygdaloidal	Pl	Kf, Mt	Pl	Chl, Cal, Ep	Pl has sieve texture. Chlorite in matrix is high. phenocrysts value < 10. Cal is amygdales
KH2	Basaltic andesite	Vitrophyric	Pl	Kf, Mt	Chl	Chl, Cal	Matrix is cryptocrystalline and glassy
RK3	Basaltic andesite	Porphyric	Pl, Kf, Cpx	Hbl, Qtz	Pl	Cal, Chl, Ep	
SK1*	Trachy-andesite	Porphyric, vesicular	Kf, PL	Hbl, Mt	Kf, Pl, Mt	Clay, Ep (rare)	Pl and Kf have sieve texture. Hbl is replaced by opacities. mafic mineral value < 10
SK2*	Trachy-andesite	Porphyric, vesicular	Kf, PL	Hbl, Mt	Kf, Pl, Mt	Clay, Sc	
SK3*	Basaltic andesite	Porphyric	Cpx, Pl	Mt	Pl, Cpx, Mt	Act, Ep, Chl	Cpx is zoning
SK4*	Basaltic andesite	Porphyric	Pl, Cpx	Mt	Pl, Cpx, Mt	Act, Ep, Chl	
SS1*	Trachy-andesite	Trachyte-porphyric	Kf, Qtz, Hbl	Pl, Tit, Mt	Bt	Cal, clay, Ep	Hbl is replaced by opacite

Group 2 is showed by star (*). Mineral abbreviations from Kretz (1994). Cal: calcite; Pl: plagioclase; Kf: K-feldspar; Mt: magnetite, Hbl: hornblende; Ep: epidote; Ab: albite; Act: actinolite; Chl: chlorite; Ze: zeolite; Tit: titanite (sphene).

References

Alavi, M., 1994. Tectonics of Zagros Orogenic belt of Iran, new data and interpretation. Tectonophsics 229, 144–149.

Ayers, J., 1998. Trace elements modelling of aqueous fluid–peridotite interaction in mantle wedge of subduction zones. Contrib. Miner. Petrol. 132, 390–404.

Azizi, H., Moinevaziri, H., Mohajjel, M., 2005. Pull-a Part Basin a Tectonic Setting for Cretaceous Volcanic Rocks, 8th, Geology Symposium of Iran, (in Persian).

Azizi, H., Moinevaziri, H., Mohajjel, M., Yagobpoor, A., 2006. PTt path in metamorphic rocks of the Khoy region (northwest Iran) and their tectonic significance for Cretaceous–Tertiary continental collision. J. Asian Earth Sci. 27, 1–9.

Azizi, H., 2002. Petrography, petrology and geochemistry of the Khoy metamorphic rocks. Ph.D. Thesis. University of Tarbiat Moalem, Tehran, Iran, 255 pp. (in Persian).

Berberian, F., Berberian, M., 1981. Tectono-plutonic episodes in Iran. American Geophysical Union. Geodynamics series 3, pp. 5–32.

Berberian, M., 1995. Master blind thrust faults hidden under the Zagros folds: active basement tectonics and surface morphotectonics. Tectonophysics 241, 193–224.

Berberian, M., King, G.C.P., 1981. Toward a paleogeography and tectonic evolution of Iran. Can. J. Earth Sci. 18, 210–265.

Blourian, G.H., 1994. Petrology of Tertairy volcanic rocks in the north of Tehran. M.Sc. Thesis. University of Tarbiat Moalem, Tehran, Iran, 145 pp.

Braud, J., 1987. La suture du Zagros au niveau de Kermanshah (Kurdistan tranien): reconstitution paléogéographique, évolution géodynamique,magmatique et structurale. Thèse. Université Paris-Sud, 489 pp.

Brenan, J.M., Shaw, H.F., Phinney, D.L., Ryerson, F.J., 1995. Rutile–aqueous fluid partitioning of Nb, Ta, Hf, Zr. U and Th: implications for high field strength element depletions in island-arc basalts. Earth Planet. Sci. Lett. 128, 327–339.

Chung, S.L., Wang, K.L., Crawford, A.J., Kamenetsky, V.S., Chen, C.H., Lan, C.Y., Chen, C.H., 2001. High-Mg potassic rocks from Taiwan: implications for the genesis of orogenic potassic lavas. Lithos 59, 153–157.

Eftekharnejad, J., 1981. Tectonic division of Iran with respect to sedimentary basins. J. Iran. Petrol. Soc. 82, 19–28 (in Persian).

Ghasemi, A., Talbot, C.J., 2006. A new tectonic scenario for the Sanandaj–Sirjan Zone (Iran). J. Asian Earth Sci. 26, 683–693.

Ghazi, A.M., Hassanipak, A.A., 1999. Geochemistry of sub-alkaline and alkaline extrusive from Kermanshah Ophiolite, Zagros suture zone, western Iran: implications for Tethyan plate tectonics. J. Asian Earth Sci. 17 (3), 319–332.

Hofmann, A.W., 1988. Chemical differentiation of the earth: the relation between mantle, continental crust and oceanic crust. Earth Planet. Sci. Lett. 90, 297–314.

Hofmann, A.W., Jochum, K.P., Seufert, M., 1986. Nb and Pb in oceanic basalts: new constraints on mantle evolution. Earth Planet. Sci. Lett. 79, 33–45.

Irvine, T.N., Baragar, W.R.A., 1971. A guide to the chemical classification of the common volcanic rocks. Can. J. Earth Sci. 8, 523–548.

Keppler, H., 1996. Constraints from partitioning experiments on the composition of the subduction zone fluids. Nature 380, 237–240.

Kretz, R., 1994. Metamorphic Crystallization. John Wiley and Sons, England, p. 507.

Lippard, S.J., Shelton, A.W., Gass, I.G., 1986. The ophiolite of northern Oman. Geol. Soc. Lond. Memoir 11, 178.

McDonough, W.F., Sun, S.S., Ringwood, A.E., Jagoutz, E., Hofmann, A.W., 1992. Potassium, Rubidium, and Caesium in the Earth and Moon and the evolution of the mantle of the Earth. Geochim. Cosmochim. Acta 56, 1001–1012.

McDonough, W.F., Sun, S.S., 1995. Composition of the Earth. Chem. Geol. 120, 223–253.

Moayyed, M., 2001. Geochemistry and petrology of volcano-plutonic bodies in Tarum area. Ph.D. Thesis. 256 pp. (in Persian).

Mohajjel, M., Fergusson, C.L., Sahandi, M.R., 2003. Cretaceous–Tertiary convergence and continental collision, Sanandaj–Sirjan Zone, western Iran. J. Asian Earth Sci. 21, 397–412.

Mohajjel, M., Fergusson, C.L., 2000. Dextral transpression in Late-Cretaceous continental collision, Sanandaj–Sirjan zone, Western Iran. J. Struct. Geol. 22, 1125–1139.

Moinevaziri, H., 1985. Volcanisme Tértiaire et Quaternaire en Iran. Thèse d' Etat. Paris-Sud Orsay, 290 pp.

Nowroozi, A., 1971. Seismo-Tectonic of the Persian Plateau, Eastern Turkey, Caucasus and Hindu-Kush Regions. Bull. Seismol. Soc. Am. 61 (2), 317–341.

Pearce, J.A., 1983. Role of sub-continental lithosphere in magma genesis at active continental margins. In: Hawkesworth, C.J., Norry, M.J. (Eds.), Continental Basalt and Mantle Xenoliths. Shiva Publishing Limited, Cheshire, U.K., pp. 230–249.

Pearce, J.A., Baker, P.E., Harvey, P.K., Luff, L.W., 1995. Geochemical evidence for subduction Fluxes, mantle melting and fractional crystallization beneath the South Sandwich Island arc. J. Petrol. 36, 1073–1109.

Pearce, J.A., Peate, D.W., 1995. Tectonic implications of the composition of volcanic arc magmas. Annu. Rev. Earth Planet. Sci. 23, 1073–1109.

Ricou, L.E., 1994. Tethys reconstructed: plates continental fragments and their boundaris since 260 Ma from Central America to Southeastern Asia. Geodinamica Acta 7, 169–218.

Rudnick, R.L., Fountain, D.M., 1995. Nature and composition of the continental crust: a lower crustal perspective. Rev. Geophys. 32, 267–309.

Ryerson, F.J., Watson, E.B., 1987. Rutile saturation in magmas: implications for Ti–Nb–Ta depletion in island arc basalt. Earth Planet. Sci. Lett. 86, 225–239.

Sengor, A.M.C., 1984. The Cimmeride orogenic system and tectonics of Eurasia. Special Paper. Geological Society of America, 195 pp.

Sengor, A.M.C., 1990. A new model for the Late Paleozoic–Mesozoic tectonic evolution of Iran and implications for Oman. In: Robertson, A.H.F., Searle, M.P., Ries, A.C. (Eds.), The Geology and Tectonics of the Oman Region, Special Publication 49. Geological Society of London, pp. 797–831.

Sengor, A.M.C., Cin, A., Rowley, D.B., Nie, S.-Y., 1993. Space–time patterns of magmatism along the Tethyan sides: a preliminary study. J. Geol. 101, 51–84.

Sengor, A.M.C., Natal'in, B.A., 1996. Paleotectonics of Asia: fragments of a synthesis. In: Yin, A., Harrison, T.M. (Eds.), The Tectonic Evolution of Asia. Cambridge University Press, pp. 486–640.

Shahabpour, J., 2005. Tectonic evolution of the orogenic belt in the region located between Kerman and Neyriz. J. Asian Earth Sci. 24, 405–417.

Stampfli, G.M., Mosar, J., Faver, P., Pillevuit, A., Vannay, C.J., 2001. Permo–Mesozoic evolution of the western Tethyan realm: the Neo-Tethys/East-Mediterranean connection. Pre-Tethyan memoir 6: Pre-Tethyan rift/wrench basins and passive margins. Int. Geol. Correlat. Prog. 369, 51–108.

Stocklin, J., 1968. Structural history and tectonic of Iran; a review. Am. Assoc. Petrol. Geol. Bull. 52, 1229–1258.

Sun, S.S., McDonough, W.F., 1989. Chemical and isotopic systematic of oceanic basalts: implication for mantle composition and processes. In: Sunders, A.D., Norry, M.J. (Eds.), Magmatic in Oceanic Basins, Special Publication 42. Geology Society of London, pp. 313–345.

Takin, M., 1972. Iranian geology and continental drift in the Middle East. Nature 23, 147–150.

Tatsumi, Y., Hamilton, D.L., Nesbite, R.W., 1986. Chemical characteristics of fluid phase released from a subducted lithosphere and origin of arc magmas: evidence from high-pressure experiment and natural rocks. J. Volcanol. Geotherm. Res. 29, 293–309.

Taylor, S.R., McLennan, S.M., 1985. The Continental Crust: its Composition and Evolution. Blackwell, Cambridge, p. 312.

Weaver, B.L., 1991. The origin of ocean island end members composition: trace element and isotopic constraints. Earth Planet. Sci. Lett. 104, 381–397.

Zahedi, M., Hajian, J., Blourchi, H., 1985. Geology Map of Sanandaj (Scale 1:250000). Geological Survey of Iran.